International Journal of Nanomedicine

Dovepress
Taylor & Francis Group

Open Access Full Text Article

ORIGINAL RESEARCH

Engineered *E. coli* OMVs Carrying the Membrane-Binding hGC33 Fragment Precisely Target Liver Cancer and Effectively Treat Tumor

Yufei Deng[1], Bangya Yang[1], Zelan Yang[1], Hanyu Xiao[1], Yan Zou[1], Cheng Zou[1], Song Yang[1], Xi Sun[1], Yiting Wang[1], Jin Bai[1], Liaoqiong Fang[1,2], Zhibiao Wang[1,2]

[1]State Key Laboratory of Ultrasound in Medicine and Engineering, College of Biomedical Engineering, Chongqing Medical University, Chongqing, 400016, People's Republic of China; [2]National Engineering Research Center of Ultrasound Medicine, Chongqing, 401121, People's Republic of China

Correspondence: Zhibiao Wang; Liaoqiong Fang, Email wangzb@cqmu.edu.cn; lqfang06@163.com

Background: Glypican-3 (GPC3), which is a membrane-associated antigen that is overexpressed in hepatocellular carcinoma (HCC). hGC33, a humanized anti-GPC3 antibody, has been validated as a potential antibody drug with good antitumor activity by preclinical studies and the Phase II clinical trial. However, free drug usually lack good tumor penetration. Outer membrane vesicles (OMVs) that are secreted by *Escherichia coli* function as natural vectors for molecule delivery and mediators of biological signals across tissues. Our study aimed to engineer *E. coli* for use as a platform to precisely deliver the hGC33 single-chain variable fragment (hGC33-scFv) for the targeted treatment of HCC.

Methods: In this study, we utilized *E. coli BL21(DE3)* to express Hbp-hGC33-scFv fusion protein and generated *E. coli* hGC33-OMVs. After isolation and characterization, we assessed their chemotaxis toward HepG2 cells by Transwell, coimmunoprecipitation (co-IP) to confirm hGC33-GPC3 binding, and immunofluorescence (IF) to evaluate the localization of hGC33 on OMV membranes. The in vivo efficacy was assessed in BALB/c nude mice harboring HepG2 cell-derived xenografts, and tumor targeting was analyzed with Cy7-labeled OMVs and live imaging. Proliferation assays, cell cycle analysis, and Wnt pathway expression analysis were performed to elucidate the underlying mechanisms.

Results: hGC33-OMVs exhibited spherical bilayered nanostructures and displayed hGC33-scFv on their surface. hGC33-OMVs preferentially accumulated in tumors, significantly reducing tumor volume compared with controls and downregulating the proliferation markers Ki67 and PCNA. Transwell assays revealed increased tropism of hGC33-OMVs toward HepG2 cells, while Co-IP confirmed the direct interaction between hGC33 and GPC3. Meanwhile, hGC33-OMVs suppressed HepG2 cell proliferation, induced G1-phase arrest, and reduced Wnt3a, β-catenin, Cyclin D1, and C-myc expression.

Conclusion: Engineered *E. coli* hGC33-OMVs effectively target HCC via the hGC33-GPC3 interaction, inhibit tumor growth by suppressing Wnt signaling, and demonstrate potential for use as a versatile platform for antibody delivery.

Keywords: hepatocellular carcinoma, glypican-3, outer membrane vesicles, targeted therapy, Wnt signaling pathway

Introduction

Liver cancer is one of the most common malignant tumors worldwide. According to National Cancer Institute (NCI) statistics, hundreds of thousands of patients are affected by liver cancer every year, and the number of liver cancer patients is increasing annually.[1,2] Although the use of vaccines,[3] anticancer drugs,[4] and other related treatment methods[5] led to a decrease in the mortality rate of liver cancer in some areas by 2023, the global burden of liver cancer continues to increase.[1,2] Hepatocellular carcinoma (HCC) is one of the major types of liver cancer; however, effective treatment of HCC in the clinic is often limited by its high heterogeneity, and molecularly targeted therapies have little effect on patients with advanced liver cancer.[6] One manifestation of HCC is the high expression of glypican-3 (GPC3) in tumor cells, and GPC3 expression is used for clinical diagnosis or to assess malignancy.[7,8] In these cases, liver cancer cells from HCC patients exhibit greater GPC3 expression than

Received: 20 February 2025
Accepted: 13 May 2025
Published: 22 May 2025

Graphical Abstract

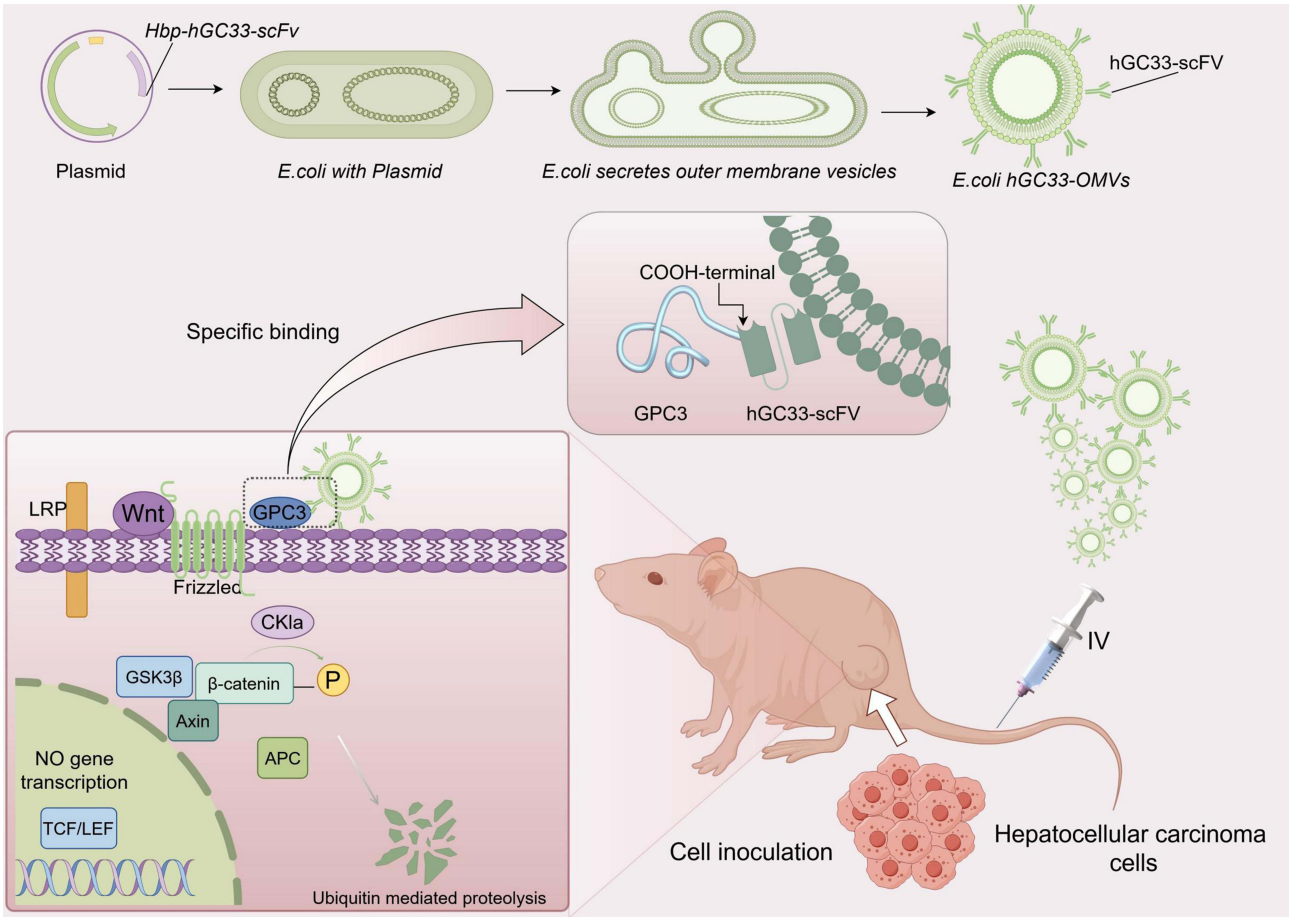

liver cells from healthy patients;[9] therefore, GPC3 is typically used as a therapeutic target for HCC. GPC3 activates classic Wnt signaling by binding to Wnt-related proteins,[10,11] thus promoting the proliferation and growth of HCC cells.[12]

Researchers have prepared a variety of antibodies that are specific for GPC3, such as the GPC3-specific human single-domain antibody (HN3) PET probe that was designed by Fayn et al[13] the YP7 antibody that specifically binds to GPC3 that was developed by Yen Phung's team,[14] the humanized monoclonal antibody hGC33 that was prepared by Ishiguro et al[15] and the HN3 antibody that was constructed by Mingqian Feng et al[16] using bacteriophages. Therefore, hGC33 can specifically recognize and bind to GPC3. hGC33 mainly inhibits the growth of HCC in tumor-bearing mice but also suppresses the proliferation of HCC cells in vitro by binding to the C-terminus of GPC3.[17] Considering these findings, we hypothesized that hGC33 may inhibit the growth of HCC by downregulating Wnt signaling pathway components through its specific interaction with GPC3. However, the binding efficiency of foreign antibodies in vivo is low. The direct delivery of antibodies to the tumor site via tools can allow these antibodies to efficiently bind to and directly act on tumor cells.

Escherichia coli outer membrane vesicles (*E. coli* OMVs) are functional vesicles that are produced by *E. coli*; these OMVs are continuously secreted from the membrane surface of *E. coli* during growth. These vesicles have spherical, lipid bilayer nanostructures with diameters typically ranging from 20 to 300 nm.[18] The interior of OMVs contains a diverse array of biological components that are derived from the parental bacteria, allowing them to perform a multitude of specific biological functions, such as stimulating immune responses, presenting antigens, and delivering

drugs in a targeted manner.[19] To more accurately enhance the functions of OMVs, some researchers have recently engineered the *Escherichia coli* autotransporter (AT) hemoglobin protease (Hbp) for use as a platform for the high-density surface display and expression of heterologous proteins on the surface of OMVs,[20,21] such as the Mycobacterium tuberculosis antigens ESAT6, Ag85B, and Rv2660c.[22,23] In the autotransporter protein display system, ATs consist of an N-terminal signal peptide, a secreted or surface-displayed passenger structural domain, and a C-terminal translocation unit polypeptide;[21] this structure allows for the display of heterologous proteins on the cell surface via gene fusion. We used a similar approach, utilizing the passenger domain structure of the Hbp to heterologously present hGC33-scFv via a prokaryotic expression vector, and we prepared OMVs carrying Hbp-hGC33-scFv (*E. coli* hGC33-OMVs).

Here, we established a platform in which hGC33-scFv was localized to the OMV membrane surface, and our findings were compared with those of nongenetically modified *E. coli* outer membrane vesicles (wt-OMVs); the results revealed that *E. coli* hGC33-OMVs exhibited significant abilities to target liver tumors in holomatous mice. Additionally, we explored whether *E. coli* hGC33-OMVs could specifically bind to and recognize the antigenic protein GPC3 on the membrane surface of HepG2 cells and inhibit HepG2 cell cycle progression and cell proliferation by modulating the Wnt signaling pathway. This study confirms the utility of hGC33-OMVs and offers novel insights into the synergistic targeting of outer membrane vesicles to GPC3 to treat tumors, and these findings have potential to transform the therapeutic strategies that are used to treat HCC.

Materials and Methods

Materials

Dulbecco's modified Eagle's medium (DMEM), 0.25% trypsin (GIBCO, USA) and fetal bovine serum (CLARK Bioscience, USA) were used. The following antibodies were used: anti-OmpC monoclonal antibody (Thermo Fisher Scientific, USA), anti-OmpA monoclonal antibody (Affinity, USA), anti-Myc tag monoclonal antibody, anti-recombinant GAPDH antibody, anti-Actin antibody, anti-PCNA Rabbit monoclonal antibody, anti-Ki67 Rabbit monoclonal antibody (Beyotime, CHN), anti-Wnt3a monoclonal antibody (Abcam, USA), gold-labeled sheep anti-rabbit IgG (10 nm) (Solarbio Technology, UK), anti-Wnt3a monoclonal antibody, anti-Cyclin D1 monoclonal antibody, anti-C-myc monoclonal antibody, and anti-β-catenin monoclonal antibody (MedChemExpress, America). The following reagents were used: chlorpromazine (MedChemExpress, USA), the Quantinova SYBR PCR MIX Kit (QIAGEN, German), the Enhanced BCA Protein Assay Kit, the Myc-tag Protein IP Assay Kit with Magnetic Beads, the BeyoClick^{TM} EdU Cell Proliferation Kit with AF555 and the SDS-PAGE Gel Quick Preparation Kit (Beyotime, CHN), the YSFluor^{TM} 488 Goat Anti-Mouse lgG(H+L), the YSFluor^{TM} 594 Goat Anti-Mouse lgG(H+L) (Yeasen, CHN). All the other analytical grade chemicals, reagents, and solvents were obtained from standard suppliers and were ready to use without further purification.

Cell Lines and Experimental Animals

The human liver cancer cell line HepG2 (BC-C-HU-024) was purchased from Biochannel. The cells were cultured in incubators with an atmosphere of humidified 5% CO_2 and grown in DMEM supplemented with 10% (vol/vol) FBS at 37 °C. BALB/c nude mice, weighing approximately 20–22 grams and 4 weeks of age, were purchased from Chengdu Enswell Biotechnology Co., Ltd., and housed in an IVC facility. All the animal care and treatment procedures were conducted in accordance with the guidelines set forth by Chongqing Medical University. All the experimental protocols were reviewed and approved by the Institutional Animal Care and Use Committee of Chongqing Medical University (Approval Number: IACUC-CQMU-2024-07067).

Strains and Culture Conditions

The present study was conducted in LB growth medium supplemented with 50 μg/mL kanamycin and 0.2% glucose, and the bacteria were incubated at 37 °C. The bacterial strains that were utilized were *BL21 (DE3)/pET28a-Hbp-hGC33* and *BL21 (DE3)/pET28a*. The appropriate IPTG concentration was used, and the experiments were conducted at 16 °C.

Construction of Plasmids

According to the collation of Nakano et al[15] we obtained relevant sequence information for GC33. The sequences of the heavy chain variable region (VHk) and light chain variable region (VLa) of the humanized monoclonal antibody hGC33 were linked together with a flexible peptide (GGGGSGGGGSGGGGS) to form the single chain antibody hGC33-scFv. Myc (EQKLISEEDL) was fused to the C-terminus of hGC33-scFv, and then, this sequence was inserted between the signal peptide (SP) and the passenger domain (passenger) of the full-length Hbp protein. The Hbp-hGC33-scFv codon sequence was cloned and inserted into the expression vector pET28a between the *NcoI* and *NcoII* restriction sites. The recombinant expression plasmid was named *pET28a-Hbp-hGC33-scFv.* Then, *pET28a-Hbp-hGC33-scFv* was transfected into *E. coli BL21 (DE3)*. Gene sequencing of the recombinant expression strain *BL21(DE3)/pET28a-Hbp-hGC33-scFv* was performed by Bio-Sanitary Industry Company (Shanghai, China). Moreover, the empty plasmid *E. coli BL21 (DE3)/ pET28a* was constructed and used as an experimental control.

OMV Isolation, Extraction, and Characterization

The wild-type *E. coli* strains BL21 (DE3) and *BL21 (DE3)/pET28a-Hbp-hGC33* were cultivated in LB broth supplemented with kanamycin (50 μg/mL) and glucose (0.2%) at an OD600 of 0.4. Subsequently, 0.1 M isopropyl-β-D-1-thiogalactopyranoside (IPTG) was added to a final concentration of 5 mM to induce protein expression. The temperature was reduced to 16 °C, and induction was allowed to proceed for one hour. To separate and purify the OMVs, the sample was subjected to centrifugation at 5,000 × g for 15 minutes at 4 °C to remove the bacterial precipitate. The supernatant was then filtered through 0.45-μm and 0.2-μm filters. The filtered solution was then filtered again through a 100-kDa ultrafiltration tube to concentrate the OMVs, which were collected by centrifugation at 150,000 × g for three hours at 4 °C (Beckman Coulter). The OMVs were imaged via transmission electron microscopy (TEM) (Hitachi, Japan) to determine their morphology. NanoSight (Malvern, UK) nanoparticle tracking analysis (NTA) was performed to determine the size distribution of the OMVs. Additionally, Western blotting was used to measure the expression of OmpA and OmpC, which are outer membrane proteins of bacteria.

Immunogold EM

The wt-OMVs and hGC33-OMVs were diluted in PBS and subjected to centrifugation at 150,000 × g for 3 hours to remove the supernatant. The pellets were then fixed with 4% paraformaldehyde for 24 hours and incubated with 1% BSA to block the copper grids. The grids were incubated with 10-nm gold-labeled goat antibodies against rabbit antigens to label the OMVs, incubated with uranyl acetate, and analyzed by transmission electron microscopy.

In vitro Chemotaxis Assay

The tendency of wt-OMVs and hGC33-OMVs to migrate toward cells was determined via the Transwell method. The cells were suspended in serum-free culture medium at a density of 5×10^5 cells/mL. A total of 400 μL of complete culture medium was added to the lower chamber, and 400 μL of complete culture medium was added to the upper chamber. A 200 μL cell suspension was added to the upper Transwell chamber, and 250 μL bacterial outer membrane vesicles were added to the lower chamber. The samples were incubated at 37 °C in a CO_2 incubator for 24 hours. The cells were stained with 1% crystal violet for 20 minutes and subsequently washed three times with PBS. After the excess moisture from the upper chamber was removed with a cotton swab, the number of cells was counted under a microscope.

In vitro Cell Proliferation Assay

The cytotoxic effects of wt-OMVs and hGC33-OMVs were determined with a CCK8 assay. HepG2 cells were seeded at a density of 5,000 cells per well in a 96-well plate and incubated in a 5% CO_2 incubator at 37 °C for 48 hours. The cells were then treated with PBS, wt-OMVs, or hGC33-OMVs in a 5% CO_2 incubator at 37 °C for 24 hours. After the incubation period, cell viability was assessed via the CCK8 assay. The absorbance at 490 nm of each well was measured.

Cell proliferation was evaluated via an EdU assay. The results demonstrated that the OMVs and hGC33-OMVs inhibited cell proliferation. Following an overnight incubation of log-phase cells in 6-well plates, the cells were treated

with wt-OMVs, hGC33-OMVs, or hGC33-OMVs+chlorpromazine for a period of 24 hours. The anti-proliferative activity was then evaluated with the EdU assay, and the results were observed under a fluorescence microscope and subsequently quantified. The data were analyzed via ImageJ.

Immunofluorescence Staining

Cells were fixed with 4% paraformaldehyde (Biosharp; BL539A) for 15 min at room temperature (RT), permeabilized with 0.1% Triton X-100 (Solarbio; T8200) for 5 min and then blocked with QuickBlockTM immunostaining blocking solution (Beyotime; P0260) for 15 min at RT. The cells were incubated with primary antibodies diluted in blocking buffer at 4 °C overnight. The following primary antibodies were used: anti-GPC3 (AF7002; rabbit; Beyotime). To detect the primary antibodies, the cells were incubated with Alexa Fluor 488 donkey anti-rabbit IgG (34206ES60; Yeasen) or Alexa Fluor 594 donkey anti-rabbit IgG (34212ES60; Yeasen) for 1 h at RT. The cells were counterstained with 4′-6-diamidino-2-phenylindole (DAPI) (Beyotime; C1006) for 5 minutes before being mounted with a laser scanning confocal microscope (LSCM; SP8 Leica, Germany).

Cell Cycle Analysis

Following an overnight incubation of log-phase cells in a 6-well plate at 37 °C, the cells were treated with wt-OMVs or hGC33-OMVs for 24 hours. Afterward, the cells were collected with ethanol and stained with the iodine propidium. The resulting single-cell suspensions were analyzed on a CytoFLEX flow cytometer (Beckman Coulter).

In vivo Targeted Evaluation in Tumor-Bearing Mice

Cy7 dye (1:1 volume ratio with OMVs) and wt-OMVs (total protein 50 μg) were incubated at 37 °C in the dark for 2 hours. Then, the mixture was ultracentrifuged at 150 000×g for 3 hours at 4 °C. The pellet was subsequently resuspended in 1 mL of PBS. Two tumor-bearing mice with good health status were injected via the tail vein with 200 μL of Cy7-labeled wt-OMVs or hGC33-OMVs. For each type of nanoparticle, a total of 50 μg were administered to the mice, and a live animal imaging system was used to determine their distribution in vivo. The mice were imaged at 1 hour postadministration.

Anti-Tumor Effects in Hormonal Mice in vivo

The inhibitory effects of wt-OMVs and hGC33-OMVs on HCC growth in vivo were determined. All the experiments were performed with BALB/c mice in a temperature-controlled room (23±2 °C) with 12 h/12 h light/dark cycles, according to the animal health regulations and guidelines of the Ethics Committee of Chongqing Medical University.

A suspension containing 5×10^6 HepG2 cells was subcutaneously injected into the left dorsal region of 5-week-old female BALB/c mice (20~22 g). This procedure established a xenograft model of human HCC in BALB/c mice. The formation of tumors was observed, and the volume was recorded when the tumor volume reached approximately 30–50 mm^3. Then, the mice were randomly divided into three groups, with 12 mice in each group. The mice were administered PBS (200 μL) or hGC33-OMVs (dose of 2.5 μg in 200 μL), and the control group received 2.5 μg of wt-OMVs in the same volume. Each treatment was repeated every two days for a total of four administrations. The weight and tumor size of the mice were measured every two days, and the antitumor efficacy was calculated. The tumor volume was calculated via the following formula: volume = $0.5\times L\times W^2$ (where L is the longest diameter of the tumor and W is the width of the tumor perpendicular to the longest diameter). The inhibition rate was calculated with the following formula: inhibition rate = (C-T)/C × 100%, where C represents the average tumor weight of the control group and T represents the average tumor weight of the experimental group. After 2 weeks of treatment, the mice were euthanized. The tumor tissue was then processed with a 4% formalin solution, paraffin-embedded, sectioned, and stained with hematoxylin and eosin, and then, the pathological changes in the transplanted tumors were analyzed by microscopy.

Quantitative Real-Time Polymerase Chain Reaction

To evaluate the activation of signaling pathways and the expression of target genes, the effects of wt-OMVs and hGC33-OMVs on inhibiting gene expression in HCC cells were evaluated. Total RNA was extracted via TRIzol reagent

(Invitrogen; 98597501), and cDNA was synthesized via a reverse transcription kit (Vazyme; R323-01). Fluorescence real-time quantitative PCR was then performed using the resulting cDNA. The reaction conditions were as follows: 95 °C for 5 minutes, 95 °C for 10 seconds, 55 °C for 20 seconds, and 72 °C for 20 seconds. Forty cycles were performed, and a melting curve was generated. The Ct values of each group were used to calculate 2-ΔΔCt.

Western Blotting

To evaluate the activation of signaling pathways and the expression of target molecules, cells were cultured in 6-well plates overnight and treated with wt-OMVs, hGC33-OMVs, or hGC33-OMVs+chlorpromazine. The cells were treated for 24 hours, after which samples were collected, proteins were extracted, and protein concentrations were determined. The protein concentrations were determined via a BCA protein reagent kit (Beyotime, China). Then, protein samples were separated by 10% SDS–PAGE, transferred to PVDF membranes, and blocked with 5% BSA. The primary antibody (diluted 1:1000) was incubated at 4 °C overnight, and the secondary antibody (diluted 1:2000) was incubated at room temperature for 1 hour. The protein bands were visualized with a hypersensitive ECL chemiluminescence kit (G2020; Servicebio; China), and the images were analyzed via a gel imaging system. GAPDH and Actin were used as reference controls.

Data Analysis and Statistics

The data are presented as the mean ± standard deviation (SD) and were analyzed using GraphPad Prism 8.0 for variance. ANOVA was used for statistical analysis, and independent-samples paired t tests were used for pairwise comparisons. A p value of less than 0.05 was considered to indicate a statistically significant difference.

Results

Characterization of E. coli wt-OMVs and E. coli hGC33-OMVs

The variable region sequence of hGC33 was obtained from the literature,[15] and a Myc tag was introduced at the C-terminus. The hGC33-scFv/Myc single-chain antibody sequence (1−243 aa) was inserted between the signal sequence and the passenger domain sequence of Hbp, ultimately yielding the Hbp-hGC33-scFv/Myc fusion gene sequence (Supplementary Figure 1). This synthesized gene fragment was subsequently inserted into the pET28a expression plasmid, which was subsequently transformed into *E. coli BL21(DE3)*, and the transformed *E. coli* were screened in LB medium supplemented with kanamycin to select for the engineered *E. coli* (Figure 1a); additionally, wild-type *E. coli* was generated by transforming the empty vector pET28a into *E. coli BL21(DE3)* following the same method. The wt-OMVs and hGC33-OMVs were isolated and obtained from *E. coli* LB-conditioned liquid medium by differential centrifugation and ultrafiltration (Figure 1a and f). We examined the fusion proteins via immunocolloid gold, and immunoelectron microscopic analysis of both bacteria and their OMVs revealed that immunocolloid gold particles were present on the surfaces of the bacteria and vesicle membranes in the engineered group, whereas no immunocolloid gold particles were present in the control group (Figure 1b). Furthermore, the protocol for hGC33-OMV extraction was optimized (Supplementary Figure 2) to yield higher concentrations of hGC33-OMVs. As shown in the transmission electron micrograph (Figure 1c), the OMVs exhibited a uniform spherical and lipid bilayer structure. The NTA results demonstrated that the average diameter of the wt-OMVs was approximately 99.9 ± 2.6 nm, whereas that of the hGC33-OMVs was approximately 104.0 ± 6.0 nm (Figure 1d). The SDS–PAGE results (Figure 1g) indicated that the protein composition of the OMVs differed from that of the whole *E. coli* bacterial lysates. Furthermore, Western blotting analysis revealed that the molecular weights of OmpA and OmpC, which are characteristic proteins of bacterial outer membrane vesicles, were 36 kDa and 38 kDa, respectively. Additionally, the hGC33-OMVs contained a Myc-tagged, protein-tagged fusion protein, namely, Myc-Hbp-hGC33, which had a molecular weight of 173.5 kDa (Figure 1e).

Recognition and Binding of E. coli hGC33-OMVs to the HepG2 Cell Surface Receptor GPC3

To investigate the specific binding of hGC33 to GPC3, we performed immunocytolloid gold electron microscopy (Figure 2a) and demonstrated that Myc-tagged Hbp-hGC33 fusion proteins were expressed on the outer membrane

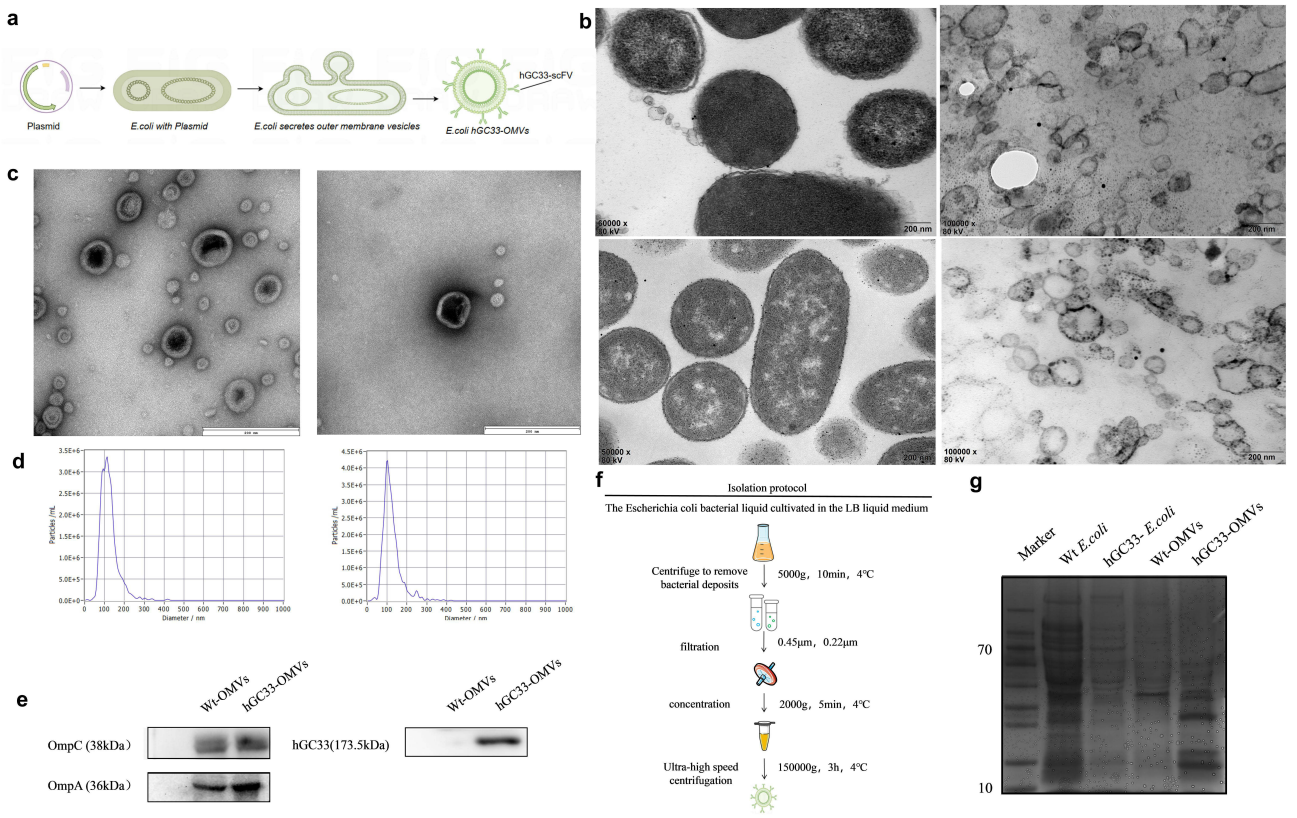

Figure 1 Display of hGC33-scFv on the membrane surface of *E. coli* OMVs. (**a**) Schematic illustration of the genetic construct used to engineer *E. coli* BL21(DE3) to display hGC33-scFv on the surface of outer membrane vesicles (OMVs). The hGC33-scFv gene was fused to the passenger domain of the autotransporter Hbp and subsequently cloned and inserted into the pET28a expression vector. (**b**) Immunoelectron microscopic analysis of engineered *E. coli* (top left) and its OMVs (top right) and wild-*type E. coli*. coli (sitting) and its OMVs (bottom right). (**c**) Transmission electron microscopy (TEM) image of hGC33-OMVs and wt-OMVs, showing uniform spherical structures with a lipid bilayer (scale bar = 100 nm). (**d**) Nanoparticle tracking analysis (NTA) of hGC33-OMVs, indicating an average vesicle diameter of approximately 104.0 ± 6.0 nm. (**e**) Western blotting analysis of hGC33-OMVs, confirming the presence of hGC33-scFv (173.5 kDa) and the bacterial outer membrane proteins OmpA (36 kDa) and OmpC (38 kDa), with a total protein amount of 3.5 μg per lane. (**f**) Protocol for OMV isolation. (**g**) Kaumas Brilliant Blue analysis of bacterial lysates and OMV preparations.

surface of hGC33-OMVs. The Transwell assay is a common method that is used to evaluate the effects of stimulants on cell migration and chemotaxis. Therefore, to investigate whether cells tend to migrate toward hGC33-OMVs due to the specific recognition and targeting of the HepG2 surface antigen GPC3, we evaluated the tropism between cells and hGC33-OMVs by assessing the number of cells that entered the lower compartment during OMV and HepG2 cell coculture; this experiment was performed without the interference of chemokines, such as serum. Compared with wt-OMVs, hGC33-OMVs exhibited a significantly stronger ability to converge with cells ($p < 0.001$) (Figure 2f).

We subsequently labeled hGC33-OMVs with DiI and incubated them with the cells for 10 minutes, 20 minutes, 40 minutes, or 1 hour. After washing with PBS, the cells were stained with DAPI. As expected, inverted fluorescence microscopy revealed that the OMVs could reach the vicinity of the cell membrane as early as 10 min after the start of incubation, and the degree of interaction between cells and OMVs increased with time, peaking at 1 h (Figure 2b). These findings suggest that OMVs can reach the cell membrane in a short time, and, through the specific binding of hGC33 to GPC3, hGC33-OMVs aggregate on the cell membrane surface. We also observed the binding of wt-OMVs and hGC33-OMVs to the cell membrane under the same conditions after 1 hour of coincubation. Merged images (Figure 2c) and fluorescence colocalization visualization analysis (Figure 2d and e) revealed that hGC33-OMVs could localize to the cell membrane surface, resulting in merged orange fluorescence, whereas wt-OMVs hardly bound to the cell membrane surface.

To further verify whether the specific binding of hGC33 to GPC3 occurred in a shorter time, hGC33-OMVs were coincubated with cells for 1 h, the cell precipitates were collected and lysed, and immunoprecipitation was performed with anti-Myc magnetic beads. The results of coimmunoprecipitation of Myc-hGC33 with anti-GPC3 antibodies were assessed by immunoblotting (IB) for GPC3; the results revealed the presence of a band in Lane 4 of the IP group that had

https://doi.org/10.2147/IJN.S513508

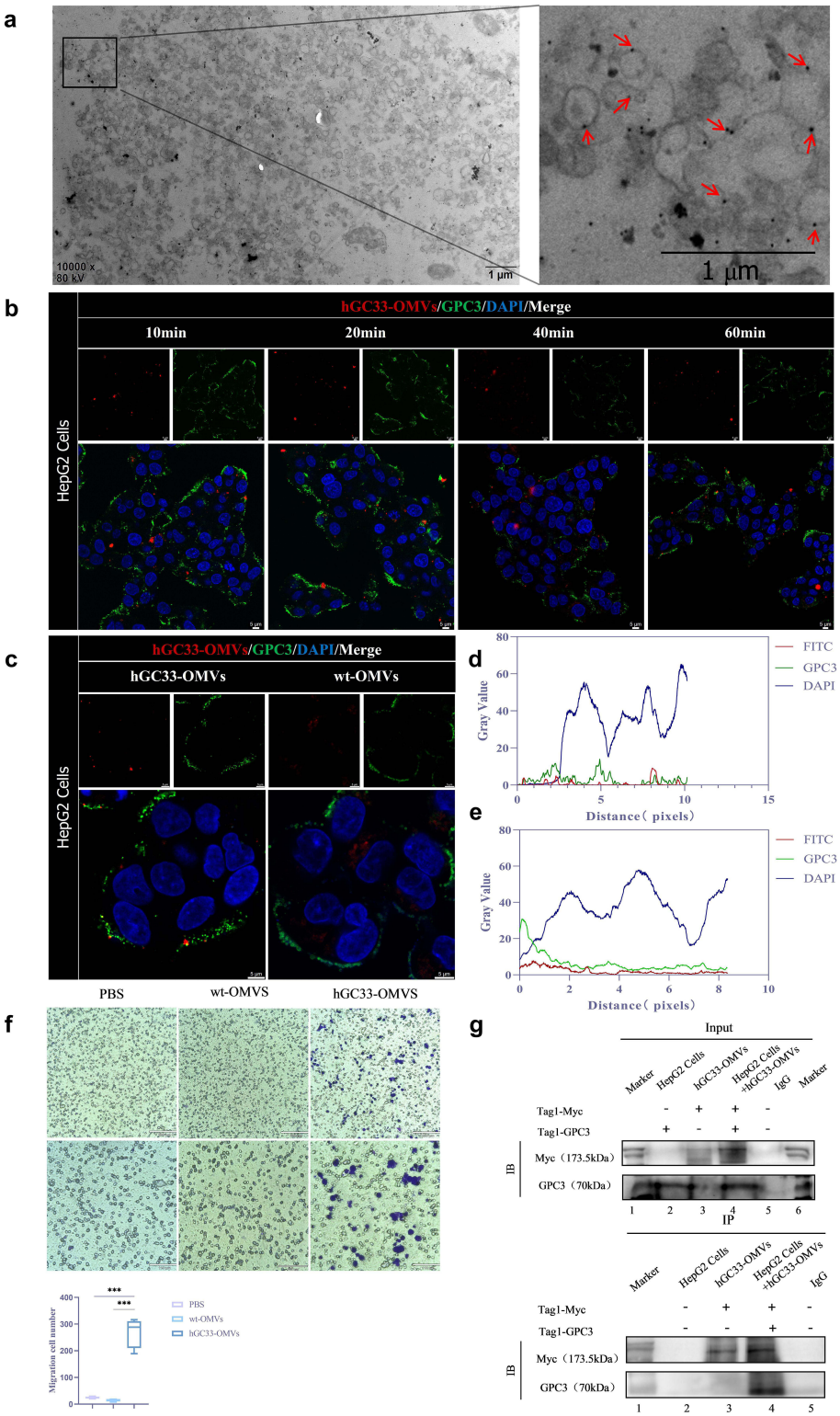

Figure 2 Specific Recognition and Binding of hGC33-OMVs to GPC3. (**a**) Fluorescence microscopy images showing the time-dependent binding of DiI-labeled hGC33-OMVs to HepG2 cells. Images were captured at 10, 20, 40, and 60 min postincubation. Nuclei were stained with DAPI (blue), and the cell membranes were labeled with FITC (green). The merged images show the colocalization of hGC33-OMVs (red) with cell membranes over time, indicating rapid and specific binding. Scale bar = 10 μm. (**b**) Fluorescence microscopy analysis of the binding of hGC33-OMVs to HepG2 cells. The cells were incubated with DiI-labeled hGC33-OMVs or wt-OMVs for 1 hour. Nuclei were stained with DAPI (blue), and GPC3 was labeled with FITC (green). Merged images showing the specific colocalization of hGC33-OMVs with GPC3 on the cell membranes. Scale bar = 10 μm. (**c**) Immunofluorescence analysis of wild-type OMVs (wt-OMVs) and hGC33-OMVs coincubated with HepG2 cells for 1 hour, with the visual results presented in (**d** and **e**), respectively. (**f**) Transwell assay analysis of the potential chemotactic effects of wt-OMVs and hGC33-OMVs on HepG2 cells (***$p < 0.0001$). (**g**) Coimmunoprecipitation (co-IP) analysis confirming the specific interaction between hGC33 and GPC3. Lysates from HepG2 cells incubated with hGC33-OMVs were immunoprecipitated with an anti-Myc antibody, followed by Western blotting with an anti-GPC3 antibody. The results revealed specific the binding of hGC33 to GPC3.

a molecular weight of approximately 70 kDa. In contrast, Lanes 2 and 3 and the IgG group presented no band of this molecular weight (Figure 2g). In other words, when the cells were coincubated with hGC33-OMVs, the two bound, but no discernible bands were observed in the cell or hGC33-OMV groups. These findings indicate that an interaction occurs between the Myc-hGC33 protein and the GPC3 protein and that hGC33 specifically binds to the GPC3 molecules on the surface of the HepG2 cell membrane.

E. coli hGC33-OMVs Regulate HepG2 Cell Proliferation by Interacting with the Surface Receptor GPC3

To determine whether hGC33-OMVs inhibit HCC cell growth, we examined the inhibition of HepG2 cell growth. First, we performed a CCK8 assay and determined that the optimal dose of hGC33-OMVs for inhibiting cell viability was 12.5 μg/mL (Figure 3a and b), and we found that hGC33-OMVs significantly reduced the number of HepG2 cells and inhibited the proliferation of HepG2 cells compared with wt-OMVs. Importantly, the results of the EdU proliferation assay (Figure 3d) also revealed that hGC33-OMVs had a stronger inhibitory effect on cell proliferation than wt-OMVs. Ki67 and proliferating cell nuclear antigen (PCNA) are the most commonly used markers of cell proliferation as well as markers related to cell cycle progression, and their expression levels reflect cell proliferation. Western blotting analysis of OMV-treated HepG2 cells revealed that PCNA protein expression was reduced in cells that were treated with hGC33-OMVs (Figure 3e). Concurrently, different OMVs were incubated with HepG2 cells. The cells were washed three times with PBS and stained with DAPI to label the nuclei. Observations were made under an inverted fluorescence microscope. The results indicated that, under the same culture conditions, cells that were treated with hGC33-OMVs presented significantly lower red fluorescence than those that were treated with wt-OMVs did (Figure 3f), suggesting that hGC33-OMVs can reduce the expression of Ki67 in HepG2 cells. In addition, at the mRNA level, we found that the expression of Ki67 and PCNA was also significantly reduced in hGGC33-OMV-treated cells, as shown by qRT–PCR (Figure 3c).

To further illustrate that the cytostatic effect was a consequence of the crosstalk between hGC33 and the cell surface membrane protein GPC3, cells were treated with the vesicle blocker chlorpromazine,[24] which is a potent inhibitor of clathrin-mediated endocytosis that blocks the binding between vesicles and cells.[25] After cells were treated with wt-OMVs, hGC33-OMVs, and hGC33-OMVs in the presence of chlorpromazine for 24 hours, the results of the EdU assay (Figure 4a) demonstrated that the inhibitory effect of hGC33-OMVs on cell proliferation was significantly diminished when chlorpromazine was added, resulting in a lower degree of inhibition than that observed following treatment with wt-OMVs. This may be attributed to the fact that OMVs possess a certain degree of intrinsic cytotoxicity.[26] The hGC33-OMV group demonstrated the strongest ability to inhibit cell proliferation, suggesting that hGC33-OMVs regulate HepG2 cell proliferation by binding to the cell membrane surface after recognition. Similarly, consistent with the Western blotting results (Figure 4b), hGC33-OMVs significantly reduced the intracellular protein expression of PCNA, and a subsequent increase in the levels of this protein was observed after the addition of chlorpromazine. We subsequently compared the protein expression levels of β-catenin, C-myc, and Cyclin D1, which are associated with the Wnt signaling pathway, under various OMV treatment conditions. Both the q-PCR (Figure 4c) and Western blotting (Figure 4d) results demonstrated that the protein levels of Cyclin D1, C-myc, and β-catenin in the hGC33-OMV treatment group were significantly lower than those in the PBS control group. These findings suggest that hGC33-OMVs may suppress the expression of these proteins. The presence of vesicle inhibitors attenuated this inhibitory effect, which may suggest that hGC33-OMVs can regulate the Wnt signaling pathway, which is associated with tumor growth, by binding to GPC3 on the surface of HepG2 cells, thereby inhibiting the proliferation of these cells. In conclusion, these findings may indicate that hGC33-OMVs can inhibit cell proliferation via cell surface recognition.

E. coli hGC33-OMVs Regulate the Wnt Signaling Pathway to Inhibit HepG2 Cell Proliferation

GPC3 can promote Wnt/β-catenin signaling pathway activation by binding to Wnt-related proteins, thereby promoting the proliferation of HCC cells.[12] To elucidate the molecular mechanisms underlying the inhibitory effect of hGC33-OMVs on HepG2 cell proliferation, we investigated the cell cycle progression of HepG2 cells that were treated with wt-

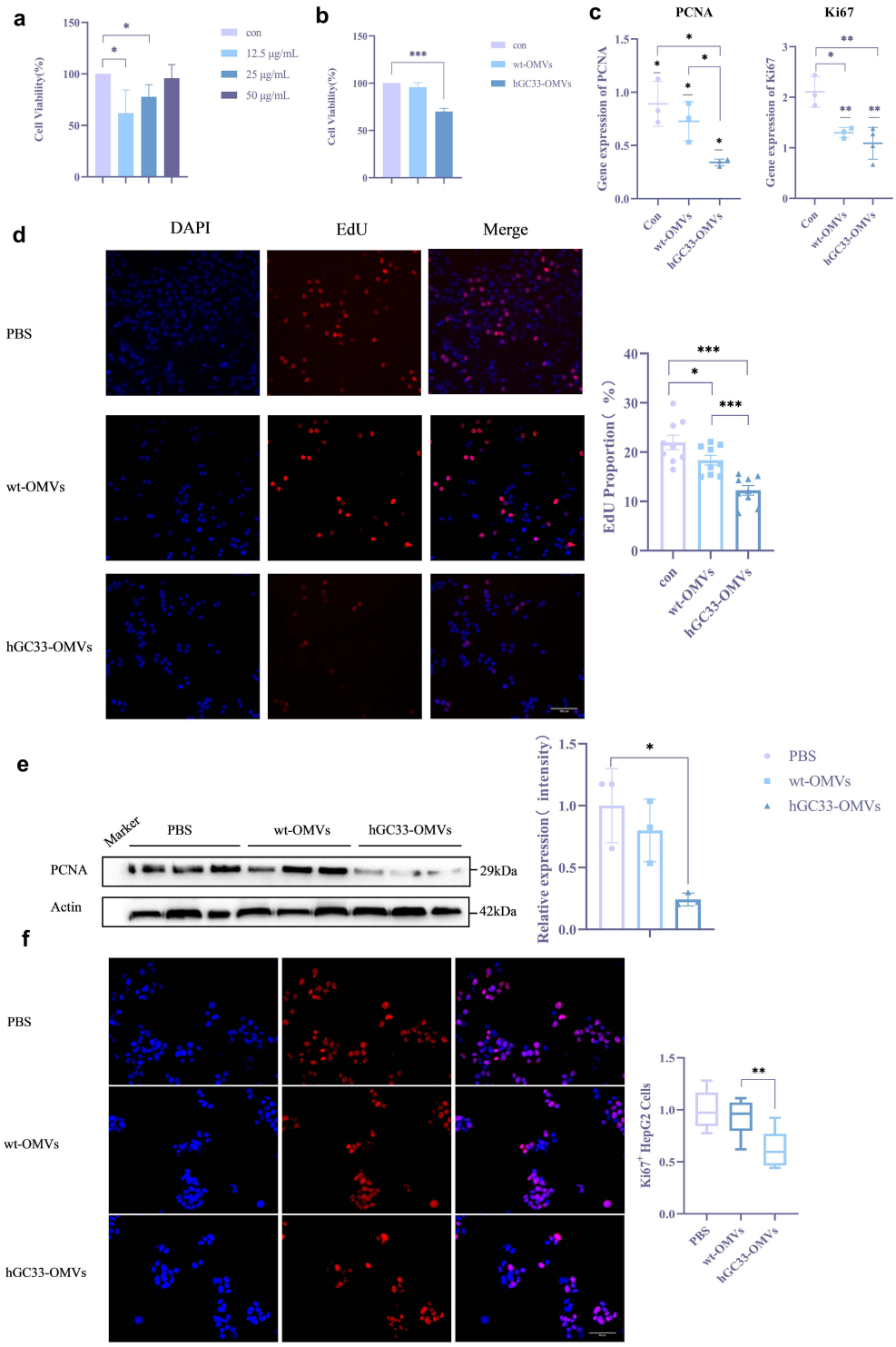

Figure 3 Inhibitory effect of hGC33-OMVs on HepG2 cells. (**a**) Cells were treated with various concentrations of hGC33-OMVs (0, 12.5, 25, or 50 μg/mL) for 24 hours, and viability was assessed with the CCK8 assay. The data are presented as the means ± SDs (n = 3). Statistical significance was determined by one-way ANOVA (*P < 0.05). (**b**) Cells were treated for 24 hours, and viability was measured with the CCK8 assay. The data are presented as the means ± SDs (n = 3). Statistical significance was determined by one-way ANOVA (***P < 0.001). (**c**) Ki67 and PCNA gene expression levels in OMV-treated HepG2 hCC cells were measured by qRT–PCR and normalized to those of GAPDH. The data are presented as the means ± SDs (n = 3). Statistical significance was determined by one-way ANOVA (*P < 0.05, **P < 0.01, ***P < 0.001). (**d**) EdU proliferation assay showing the inhibitory effect of hGC33-OMVs on HepG2 hCC cell proliferation. The proportion of EdU-positive cells was quantified. The data are presented as the means ± SDs (n = 3). Statistical significance was determined by one-way ANOVA (*P < 0.05, ***P < 0.001). (**e**) Western blotting analysis of PCNA protein expression in HepG2 hCC cells treated with OMVs for 24 hours. Actin was used as a loading control. Densitometric analysis of protein bands is shown below the blot. The data are presented as the means ± SDs (n = 3). Statistical significance was determined by one-way ANOVA (*P< 0.05). (**f**) Immunofluorescence analysis was performed to evaluate the expression levels of Ki67 in cells treated with OMVs. Nuclei were stained with DAPI (blue), and proliferating cells were labeled with Alexa Fluor 594 (red). Merged images show Ki67-positive cells. Scale bar = 10 μm. The data are presented as the means ± SDs (n = 9). Statistical significance was determined by one-way ANOVA (***P < 0.001).

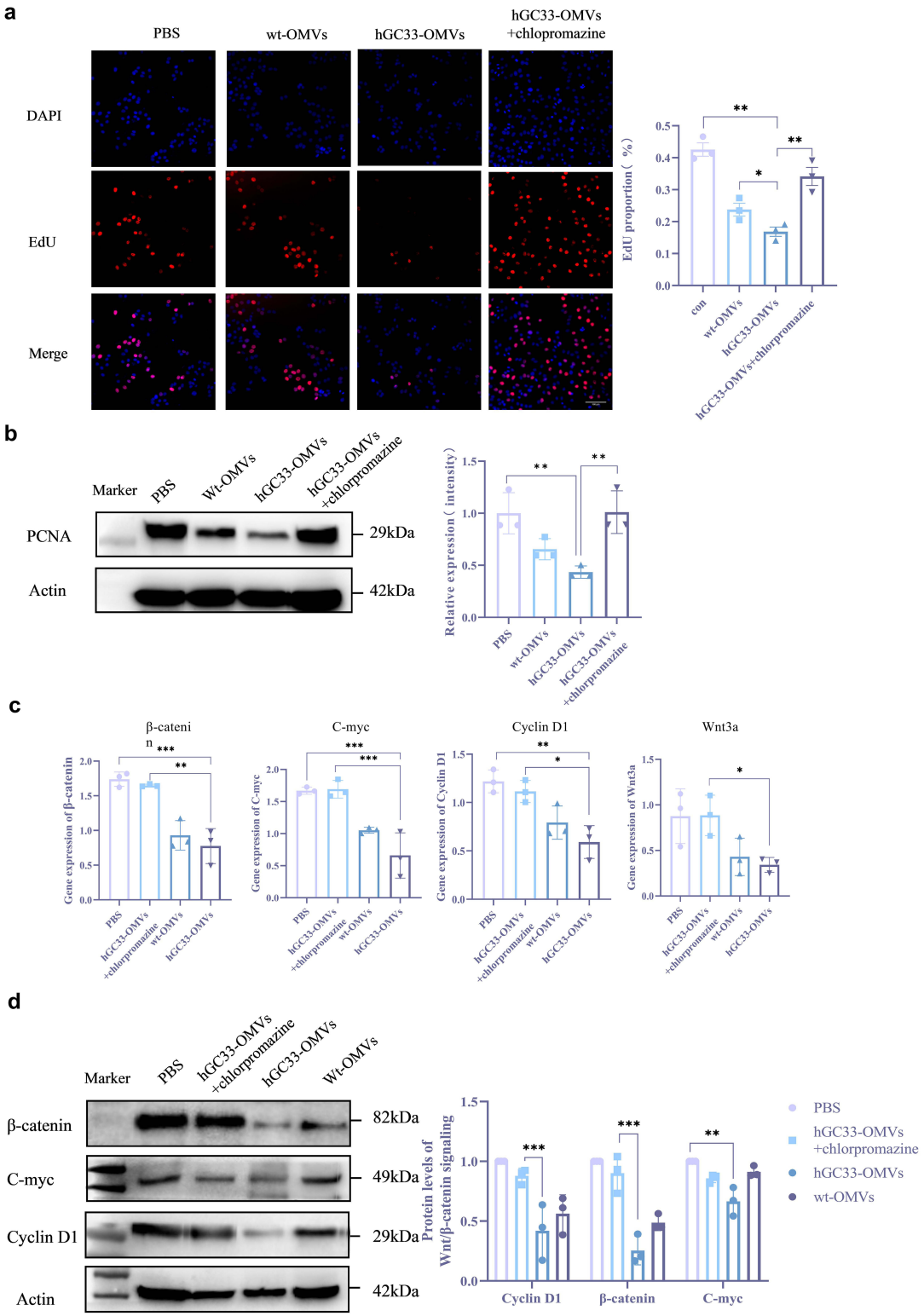

Figure 4 hGC33-OMVs regulate the Wnt signaling pathway to inhibit HepG2 hCC cell proliferation. (**a**) EdU cell proliferation analysis was performed after cells were treated with wt-OMVs, hGC33-OMVs, or hGC33-OMVs+chlorpromazine. Nuclei were stained with DAPI (blue), and proliferating cells were labeled with EdU (green). Merged images showing a reduction in the number of EdU-positive cells in the hGC33-OMV group, and chlorpromazine partially reversed this effect. Scale bar = 10 μm. The data are presented as the means ± SDs (n = 3). Statistical significance was determined by one-way ANOVA (*P < 0.05, **P < 0.01, ***P < 0.001). (**b**) Western blotting analysis of PCNA protein expression in cells treated with different OMVs. n = 3, *p <0.05; (**c**) mRNA expression of proteins involved in the Wnt signaling pathway after treatment of cells with different OMVs. Gene expression levels were normalized to those of GAPDH. (**d**) Western blotting analysis of the expression of wnt signaling pathway-related proteins in cells treated with wt-OMVs, hGC33-OMVs, or hGC33-OMVs + chlorpromazine. The data are presented as the means ± SDs (n = 3). Statistical significance was determined by one-way ANOVA (*P < 0.05, **P < 0.01, ****P < 0.001).

https://doi.org/10.2147/IJN.S513508

OMVs or hGC33-OMVs for 24 hours. In the HepG2 cell line, treatment with hGC33-OMVs significantly increased the proportion of cells in the G1 phase and decreased the proportions in the G2 and S phases (Figure 5c). In contrast, wt-OMVs had a negligible effect on cell cycle progression (Figure 5c); these results suggest that hGC33-OMVs induce cell cycle arrest at the G1 phase. These findings provide insights into the potential molecular pathways by which hGC33-OMVs inhibit HepG2 cell proliferation.

To understand the Wnt signaling pathway mechanism that are induced by the interaction of hGC33-OMVs with GPC3 in vivo, we examined the expression of Wnt/β-catenin signaling pathway-related proteins in HCC cells within the organism. In vitro, we extracted proteins from HCC tumor tissues that were treated with wt-OMVs or hGC33-OMVs. The Western blotting results revealed (Figure 5b) that the protein levels of C-myc, Cyclin D1, and β-catenin were decreased after treatment with hGC33-OMVs. Concurrently, at the mRNA level, there was a reduction in the expression levels of Wnt3a, β-catenin, C-myc, and Cyclin D1, all of which were lower than those in the wt-OMVs treatment group (Figure 5a). These findings indicate that hGC33-OMVs may modulate the Wnt signaling pathway by downregulating the expression of key pathway components at both the protein and mRNA levels, potentially impacting the proliferation and survival of HCC cells.

Targeting and Inhibition of HCC Growth by E. coli hGC33-OMVs

To verify the ability of hGC33-OMVs to target liver tumors in vivo, 5×10^5 HepG2 cells were subcutaneously inoculated into the left flank of female BALB/C nude mice, and when the tumor volume reached 30 mm^3, the mice were randomly divided into three groups: the PBS, wt-OMV, and hGC33-OMV groups. One hour after a single injection of Cy7-labeled OMVs (equivalent to 20 μg/200 μL), the distribution of the OMVs in vivo was observed via an intravital fluorescence imager. Live imaging (Figure 6h) was performed before injection (Pre) and 1 hour after injection (1 h) to assess the localization of the hGC33-OMVs. One hour after injection, imaging revealed obvious fluorescence signal enhancement, especially in the tumor area, which indicated that hGC33-OMVs could rapidly accumulate in the tumor area. These findings suggest that hGC33-OMVs have better tumor-targeting ability in vivo, which may be due to their ability to specifically recognize and bind to the GPC3 antigen on the surface of tumor cells.

To further evaluate the antitumor activity of hGC33-OMVs in vivo, HepG2 cells were subcutaneously inoculated on the left dorsal side of female BALB/C nude mice, and when the tumor volume reached approximately 30–50 mm^3, the mice were randomly divided into three groups (n=15): the PBS, wt-OMV, and hGC33-OMV groups. OMVs were injected into the tail vein (Figure 6a), and the inhibition of tumor growth in mice in each group was observed. Previously, we reported that the optimal dose of hGC33-OMVs for tumor inhibition in vivo was 2.5 μg/200 μL (Supplementary Figure 3). As shown in the figure (Figure 6b and c), both wt-OMVs and hGC33-OMVs delayed the growth of tumors compared with the control PBS, whereas hGC33-OMVs had the strongest effect on slowing tumor growth. This result occurred because wt-OMVs themselves also have some tumor inhibitory effects, which has been shown in several studies.[27] However, hGC33-OMVs more significantly inhibited HCC growth in vivo because they can specifically bind to GPC3 to target liver tumors and inhibit the Wnt signaling pathway. Compared with those of the control group, the body weights of mice in both experimental groups were lower, and the body weights of the mice that received hGC33-OMVs were greater than those of the mice that received wt-OMVs and slightly lower than those of control mice (Figure 6d). Moreover, the tumor weights in the hGC33-OMVs group were lower than those in the PBS group and the wt-OMVs group (Figure 6e and f). These findings indicate that hGC33-OMVs have lower toxicity than wt-OMVs.

The results of immunohistochemical analysis of mouse tumor tissues revealed that the rates of ki67 and PCNA positivity in the hGC33-OMV group were lower than those in the control and wt-OMV groups (Figure 6i). Consistent with these findings, qRT–PCR analysis revealed marked downregulation of Ki67 and PCNA mRNA expression in tumor tissues from the hGC33-OMV group compared with those from the control group (Figure 6g). The Western blotting results (Figure 6j) further confirmed that hGC33-OMVs decreased the protein expression of PCNA in HCC tissues. Furthermore, pathological examination of tumor tissues (Figure 6k) revealed that hGC33-OMVs induced larger areas of necrosis in liver tumors, as well as the infiltration of more inflammatory cells, suggesting that hGC33-OMVs may exert their antitumor effects, at least in part, by inducing an inflammatory response within the tumor microenvironment, leading to tumor cell death.

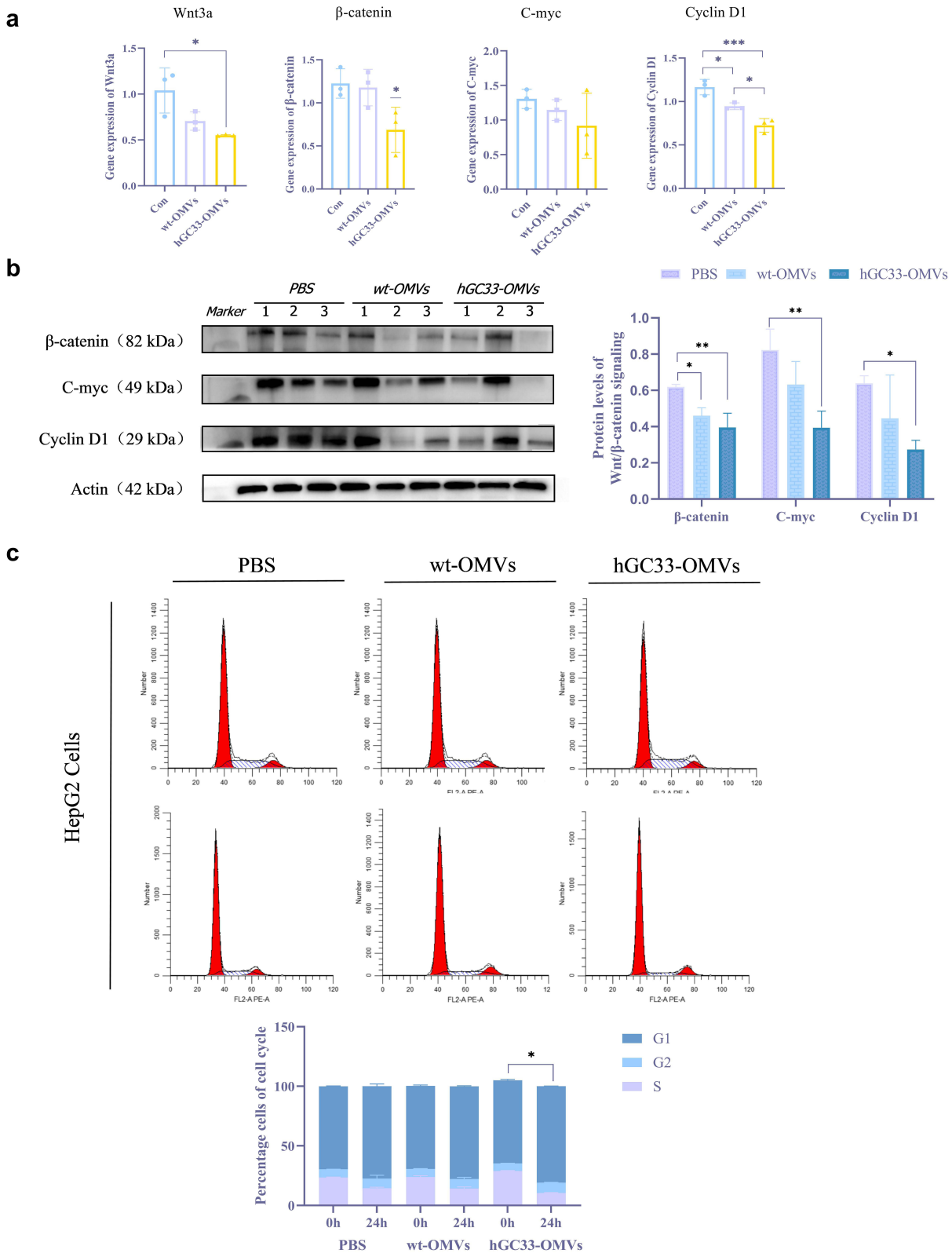

Figure 5 Effects of hGC33-OMVs on Wnt/β-catenin Signaling Pathway and Cell Cycle in HepG2 Cells. (**a**) qRT-PCR analysis of Wnt3a, β-catenin, C-myc, Cyclin D1 gene expression in HepG2 cells treated with PBS, wt-OMVs, or hGC33-OMVs for 24 hours. Data are presented as means ± SDs (n = 3). Statistical significance was determined by one-way ANOVA (*P < 0.05, ***P= 0.0009, ns=p> 0.05). (**b**) Western blot analysis of Wnt/β-catenin signaling pathway proteins (Wnt3a, β-catenin, C-myc, Cyclin D1) in HepG2 cells treated with PBS, wt-OMVs, or hGC33-OMVs for 24 hours. Actin was used as a loading control. Densitometric analysis of protein bands is shown below the blot. Data are presented as means ± SDs (n = 3). Statistical significance was determined by one-way ANOVA (*P < 0.05, **P < 0.01, ***P < 0.001). (**c**) Flow cytometry analysis of cell cycle distribution in HepG2 cells treated with PBS, wt-OMVs, or hGC33-OMVs for 24 hours. The percentage of cells in each phase (G1, S, G2) is shown. Data are presented as means ± SDs (n = 3). Statistical significance was determined by one-way ANOVA (*P < 0.05).

https://doi.org/10.2147/IJN.S513508

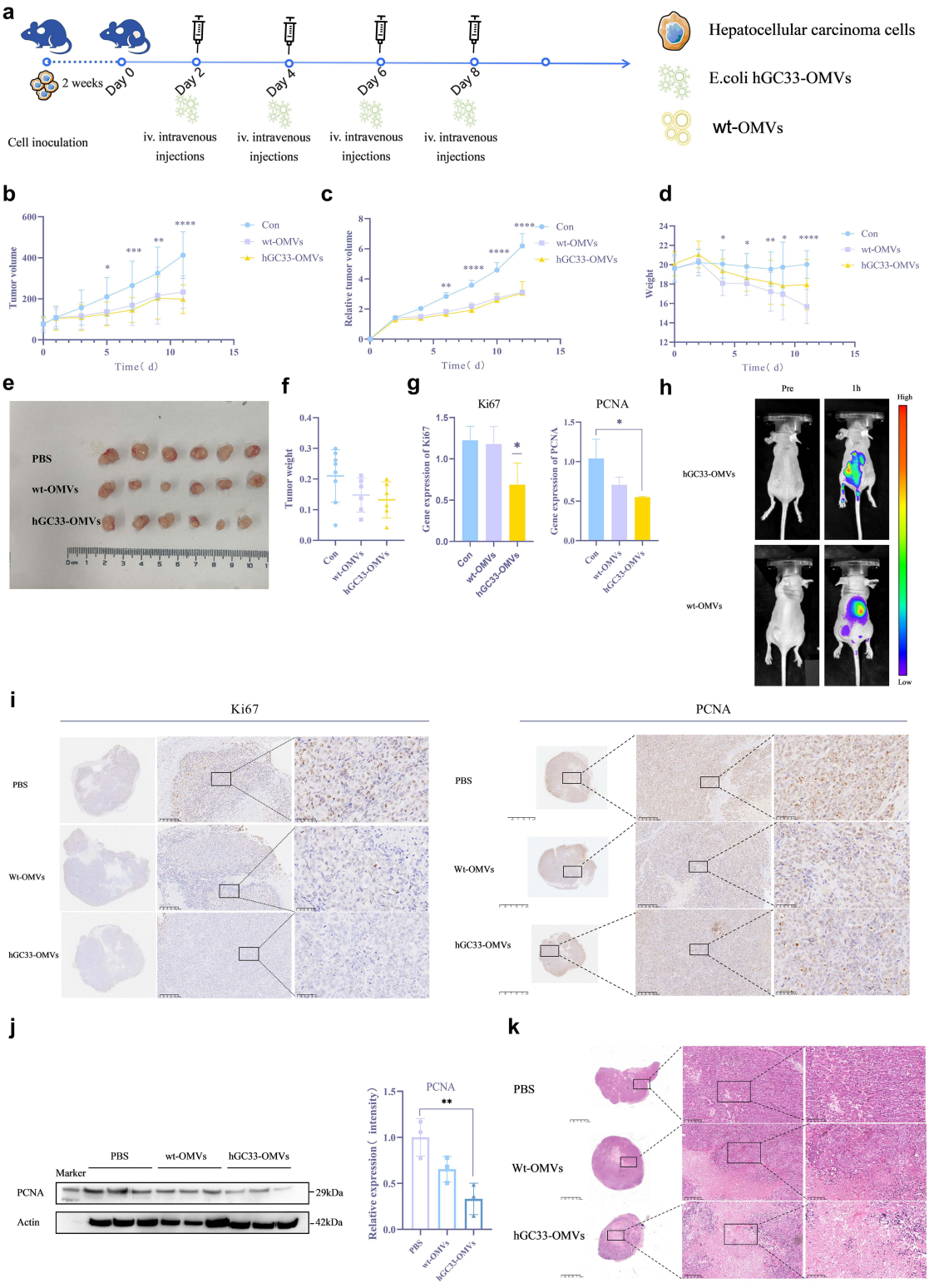

Figure 6 Effect of hGC33-OMVs on the growth of HCC graft tumors in mice. HepG2 hCC cells were inoculated into the back of each nude mouse by subcutaneous injection (n=6), and after 10 days, the mice were treated with PBS (control group), wt-OMVs or hGC33-OMVs, according to the arrangement of the animal experiments in (**a**). The tumor volumes and relative tumor volumes of the mice were measured every two days (**b** and **c**), and the body weights of the mice were measured every two days (**d**). The data are presented as the means ± SDs (n = 6). Statistical significance was determined by one-way ANOVA (*P < 0.05, **P < 0.01, ***P < 0.001, ****P < 0.0001). (**e**) Images of tumor tissues were captured and analysis of tumor weight was performed (**f**) for each group on the 15th day after initiation of the indicated treatment. (**g**) mRNA expression levels of ki67 and PCNA in tumor tissues. Gene expression levels were normalized to those of GAPDH; n = 3, *P < 0.05. (**h**) Fluorescence imaging of mice after in vivo injection of OMVs. (**i**) Immunohistochemical analysis of Ki67 and PCNA in mouse tumor tissues. (**j**) Western blotting analysis of PCNA expression in mouse tumors; n=3, **p<0.01. (**k**) H&E analysis of mouse tumor tissues.

https://doi.org/10.2147/IJN.S513508

Discussion

The global burden of liver cancer, which is one of the main causes of cancer death, continues to increase daily. According to statistics, in the past two decades, the incidence of liver cancer has increased by 53.7%, and the mortality rate has increased by 48.0%.[28] At present, liver cancer treatment has expanded from traditional methods to include immunotherapy, anticancer drugs,[29] antibody–drug conjugates (ADCs),[30] molecular targeted therapy, bacterial therapy,[31] CAR-T cell therapy,[6,32] and other methods. GPC3, which is a molecular marker of HCC, has attracted substantial attention in the field of molecular targeted therapy. Numerous research teams have dedicated efforts to exploring the potential of GPC3 for use in HCC treatment, achieving remarkable results. For example, Sun et al[33] constructed CAR-T cells that target GPC3, and the effect of exfoliated GPC3 (sGPC3) on the regulation of GPC3 on the HCC membrane surface was explored; the results revealed a new mechanism underlying immune escape by HCC. Li et al[34] also reported that CAR-T cells that target GPC3 may be developed for the treatment of HCC patients. In this study, we also focused on GPC3 as a molecular target to verify the interaction between the anti-GPC3 antibody hGC33 and GPC3, and we confirmed the potential of GPC3 for use in molecular targeted therapy for HCC.

The microenvironment of tumors is distinctly different from that of most nonmalignant tissues, which makes the tumor microenvironment a prime target for certain bacteria in bacteria-mediated cancer immunotherapy.[35,36] Facultative anaerobic bacteria can selectively accumulate in the hypoxic region of tumors[36] and drive specific T cell-mediated anticancer immunity in situ through genetic mechanisms in the tumor microenvironment,[37] as observed with *E. coli Nissle 1917(EcN)*;[38] additionally, such bacteria can be used as effective carriers of foreign genes, as observed with Salmonella typhimurium,[39] transgenic *Listeria*[40] and *E. coli Nissle 1917*,[38] which are often designed for use effective platforms to deliver antigens to tumors. Compared with other anaerobic bacteria, *E. coli* is often used as the host for heterologous protein presentation and expression because of its ease of use, low culture cost, and ease of strain optimization;[41] therefore, we chose *E. coli BL21(DE3)* as the carrier for antibody expression. However, when *E. coli* is administered to the body, the host immune system may recognize *E. coli* as a foreign pathogen, which may trigger a strong immune response, limiting its therapeutic effect.[42] Notably, the outer membrane vesicles that are secreted by *E. coli* often have lower immunogenicity. The OMVs of *E. coli*, which are naturally secreted bimolecular nanoparticles, can be selectively enriched in substances derived from bacteria, and these substances can effectively activate the natural immune signaling pathway and function as natural immune adjuvants.[43]

E. coli OMVs can be quickly recognized by and bound to immune cells because of their unique structure and heterologous identity. *E. coli* OMVs have been used to target and accumulate in tumor tissues, activate antigen-presenting cells (APCs) and adaptive immunity, induce the infiltration and accumulation of natural killer (NK) and T cells in tumor tissues, and inhibit tumors;[44] this is consistent with the fact that wt-OMVs have a certain tumor inhibition effect, as observed in our in vitro and in vivo experiments. Moreover, OMVs can be engineered for use as personalized antigen display platforms[19,45] and for the targeted delivery of drugs such as DOX,[46] 5-fluorouracil (5-FU),[41] beta-glucuronidase,[47] sorafenib[48] and PTX[49] to treat cancer. When OMVs are loaded with heterologous proteins or drugs, their natural structure can be used to quickly deliver their cargo to the target site, which greatly improves the treatment effect. Therefore, in this study, we presented hGC33-scFv on the outer membrane of *E. coli* by using the Hbp protein transport platform; thus, the OMVs that were secreted had hGC33-scFv on their membranes. Similar to the hGC33-loaded nanoparticles that were constructed by Jing Shen et al[17] hGC33-OMVs could quickly target HepG2 hCC cells and inhibit their proliferation by blocking the GPC3-Wnt signaling pathway.

We observed that when hGC33-OMVs reached the tumor site, it could inhibit the proliferation of HCC cells and down-regulate the expression of Wnt signaling pathway. This mainly depends on the fact that hGC33 antibody can induce NK cell-mediated somatic cell-dependent cytotoxicity (ADCC) effects[15] and inhibit the progress of HCC. Because hGC33 lacks a carbohydrate fraction,[15] it has a weaker ADCC effect than GC33. Nonetheless, some antitumor activity was demonstrated in a GPC3-positive cellular xenograft tumor model. This finding is supported by our finding that, in the mouse HepG2 xenograft tumor model, the tumor inhibitory effect of hGC33-OMVs, although superior to that of the wild-type vesicles, was not very significant. We speculate that this may have occurred because the surface of *E. coli*-derived outer membrane vesicles contains many virulence factors, such as LPS,[50] which stimulate immune responses via Toll-like

receptors and thus inhibit tumor cell proliferation and induce inflammatory factor release, resulting in inflammatory responses in the organism.[51] Therefore, a focus of future research may be approaches for reducing the toxicity of hGC33-OMVs to improve their safety in vivo and strategies for enhancing the ADCC effect of hGC33-OMVs; such studies would pave the way for further increasing the practical application of hGC33-OMVs in the future.

As a new targeted therapy for HCC, hGC33-OMVs not only show marked tumor-targeting and antitumor activities in vitro and in vivo but also exert good immunomodulatory effects. Future research will focus on optimizing the process of hGC33-OMV preparation, improving their safety and stability, as well as further exploring their application in combination with other treatment methods to enhance the clinical application of hGC33-OMVs and provide a new effective treatment option for HCC patients.

Ethical Statement

All the experimental protocols were reviewed and approved by the Institutional Animal Care and Use Committee of Chongqing Medical University (Approval Number: IACUC-CQMU-2024-07067). All the animal housing and experiments were conducted in strict accordance with the institutional guidelines for the care and use of laboratory animals.

Acknowledgments

This research was supported by the National Natural Science Fund by the Chinese National Science Foundation under grant number 82427901 and the Chongqing Talent Plan Project under grant number cstc2021ycjh-bgzxm0021. We would like to thank these agencies for their financial support. The graphical abstract support was provided by Figdraw.

Disclosure

The authors report no conflicts of interest in this work.

References

1. Singal AG, Kanwal F, Llovet JM. Global trends in hepatocellular carcinoma epidemiology: implications for screening, prevention and therapy. *Nat Rev Clin Oncol*. 2023;20(12):864–884. doi:10.1038/s41571-023-00825-3
2. Younossi ZM, Wong G, Anstee QM, Henry L. The global burden of liver disease. *Clin Gastroenterol Hepatol*. 2023;21(8):1978–1991. doi:10.1016/j.cgh.2023.04.015
3. Li J, Hu B, Chen Z, et al. Mn(iii)-mediated carbon-centered radicals generate an enhanced immunotherapeutic effect. *Chem Sci*. 2023;15(2):765–777. doi:10.1039/D3SC03635A
4. Kong FH, Ye QF, Miao XY, et al. Current status of sorafenib nanoparticle delivery systems in the treatment of hepatocellular carcinoma. *Theranostics*. 2021;11(11):5464–5490. doi:10.7150/thno.54822
5. Wang Y, Chen Z, Li J, et al. A paramagnetic metal-organic framework enhances mild magnetic hyperthermia therapy by downregulating heat shock proteins and promoting ferroptosis via aggravation of two-way regulated redox dyshomeostasis. *Adv Sci*. 2024;11(11):e2306178. doi:10.1002/advs.202306178
6. Llovet JM, Montal R, Sia D, Finn RS. Molecular therapies and precision medicine for hepatocellular carcinoma. *Nat Rev Clin Oncol*. 2018;15(10):599–616. doi:10.1038/s41571-018-0073-4
7. Tsuchiya N, Sawada Y, Endo I, Saito K, Uemura Y, Nakatsura T. Biomarkers for the early diagnosis of hepatocellular carcinoma. *World J Gastroenterol*. 2015;21(37):10573–10583. doi:10.3748/wjg.v21.i37.10573
8. Ishiguro T, Sugimoto M, Kinoshita Y, et al. Anti-glypican 3 antibody as a potential antitumor agent for human liver cancer. *Cancer Res*. 2008;68(23):9832–9838. doi:10.1158/0008-5472.CAN-08-1973
9. Cao L, Zhu YQ, Wu ZX, Wang GX, Cheng HW. Engineering nanotheranostic strategies for liver cancer. *World J Gastrointest Oncol*. 2021;13(10):1213–1228. doi:10.4251/wjgo.v13.i10.1213
10. Wang S, Chen N, Chen Y, Sun L, Li L, Liu H. Elevated GPC3 level promotes cell proliferation in liver cancer. *Oncol Lett*. 2018;16(1):970–976. doi:10.3892/ol.2018.8754
11. Capurro MI, Xiang YY, Lobe C, Filmus J. Glypican-3 promotes the growth of hepatocellular carcinoma by stimulating canonical Wnt signaling. *Cancer Res*. 2005;65(14):6245–6254. doi:10.1158/0008-5472.CAN-04-4244
12. Hu P, Cheng B, He Y, Wei Z, Wu D, Meng Z. Autophagy suppresses proliferation of HepG2 cells via inhibiting glypican-3/wnt/β-catenin signaling. *Onco Targets Ther*. 2018;11:193–200. doi:10.2147/OTT.S150520
13. Fayn S, King AP, Gutsche NT, et al. Site-specifically conjugated single-domain antibody successfully identifies glypican-3-expressing liver cancer by immuno-PET. *J Nucl Med*. 2023;64(7):1017–1023. doi:10.2967/jnumed.122.265171
14. Phung Y, Gao W, Man YG, et al. High-affinity monoclonal antibodies to cell surface tumor antigen glypican-3 generated through a combination of peptide immunization and flow cytometry screening. *MAbs*. 2012;4(5):592–599. doi:10.4161/mabs.20933
15. Nakano K, Ishiguro T, Konishi H, et al. Generation of a humanized anti-glypican 3 antibody by CDR grafting and stability optimization. *Anticancer Drugs*. 2010;21(10):907–916. doi:10.1097/CAD.0b013e32833f5d68

16. Feng M, Gao W, Wang R, et al. Therapeutically targeting glypican-3 via a conformation-specific single-domain antibody in hepatocellular carcinoma. *Proc Natl Acad Sci U SA*. 2013;110(12):E1083–91. doi:10.1073/pnas.1217868110
17. Shen J, Cai W, Ma Y, et al. hGC33-modified and sorafenib-loaded nanoparticles have a synergistic anti-hepatoma effect by inhibiting Wnt signaling pathway. *Nanoscale Res Lett*. 2020;15(1):220. doi:10.1186/s11671-020-03451-5
18. Chen Q, Bai H, Wu W, et al. Bioengineering bacterial vesicle-coated polymeric nanomedicine for enhanced cancer immunotherapy and metastasis prevention. *Nano Lett*. 2020;20(1):11–21. doi:10.1021/acs.nanolett.9b02182
19. Gao X, Feng Q, Wang J, Zhao X. Bacterial outer membrane vesicle-based cancer nanovaccines. *Cancer Biol Med*. 2022;19(9):1290–1300. doi:10.20892/j.issn.2095-3941.2022.0452
20. Jong WS, Soprova Z, de Punder K, et al. A structurally informed autotransporter platform for efficient heterologous protein secretion and display. *Microb Cell Fact*. 2012;11:85. doi:10.1186/1475-2859-11-85
21. Nicolay T, Vanderleyden J, Spaepen S. Autotransporter-based cell surface display in Gram-negative bacteria. *Crit Rev Microbiol*. 2015;41 (1):109–123. doi:10.3109/1040841X.2013.804032
22. Daleke-Schermerhorn MH, Felix T, Soprova Z, et al. Decoration of outer membrane vesicles with multiple antigens by using an autotransporter approach. *Appl Environ Microbiol*. 2014;80(18):5854–5865. doi:10.1128/AEM.01941-14
23. Jong WS, Daleke-Schermerhorn MH, Vikström D, et al. An autotransporter display platform for the development of multivalent recombinant bacterial vector vaccines. *Microb Cell Fact*. 2014;13:162. doi:10.1186/s12934-014-0162-8
24. Bouley R, Yui N, Terlouw A, Cheung PW, Brown D. Chlorpromazine induces basolateral aquaporin-2 accumulation via F-actin depolymerization and blockade of endocytosis in renal epithelial cells. *Cells*. 2020;9(4):1057. doi:10.3390/cells9041057
25. Erlandsson L, Ohlsson L, Masoumi Z, et al. Preliminary evidence that blocking the uptake of placenta-derived preeclamptic extracellular vesicles protects the vascular endothelium and prevents vasoconstriction. *Sci Rep*. 2023;13(1):18425. doi:10.1038/s41598-023-45830-9
26. Wai SN, Lindmark B, Söderblom T, et al. Vesicle-mediated export and assembly of pore-forming oligomers of the enterobacterial ClyA cytotoxin. *Cell*. 2003;115(1):25–35. doi:10.1016/S0092-8674(03)00754-2
27. Won S, Lee C, Bae S, et al. Mass-produced gram-negative bacterial outer membrane vesicles activate cancer antigen-specific stem-like CD8+ T cells which enables an effective combination immunotherapy with anti-PD-1. *J Extracell Vesicles*. 2023;12(8):e12357. doi:10.1002/jev2.12357
28. Hwang SY, Danpanichkul P, Agopian V, et al. Hepatocellular carcinoma: updates on epidemiology, surveillance, diagnosis and treatment. *Clin Mol Hepatol*. 2025;31(Suppl):S228–S254. doi:10.3350/cmh.2024.0824
29. Che Y, Chen G, Guo Q, Duan Y, Feng H, Xia Q. Gut microbial metabolite butyrate improves anticancer therapy by regulating intracellular calcium homeostasis. *Hepatology*. 2023;78(1):88–102. doi:10.1097/HEP.0000000000000047
30. Fu Y, Urban DJ, Nani RR, et al. Glypican-3-specific antibody drug conjugates targeting hepatocellular carcinoma. *Hepatology*. 2019;70 (2):563–576. doi:10.1002/hep.30326
31. Fleming BD, Ho M. Development of glypican-3 targeting immunotoxins for the treatment of liver cancer: an update. *Biomolecules*. 2020;10(6):934. doi:10.3390/biom10060934
32. Billingsley MM, Gong N, Mukalel AJ, et al. In vivo mRNA CAR T cell engineering via targeted ionizable lipid nanoparticles with extrahepatic tropism. *Small*. 2024;20(11):e2304378. doi:10.1002/smll.202304378
33. Sun L, Gao F, Gao Z, et al. Shed antigen-induced blocking effect on CAR-T cells targeting glypican-3 in hepatocellular carcinoma. *J Immunother Cancer*. 2021;9(4):e001875. doi:10.1136/jitc-2020-001875
34. Li D, Li N, Zhang YF, et al. Persistent polyfunctional chimeric antigen receptor T cells that target glypican 3 eliminate orthotopic hepatocellular carcinomas in mice [published correction appears in Gastroenterology. 2021;160(4):1433. doi: 10.1053/j.gastro.2021.02.025]. *Gastroenterology*. 2020;158(8):2250–2265.e20. doi:10.1053/j.gastro.2020.02.011
35. Kwon SY, Thi-Thu Ngo H, Son J, Hong Y, Min JJ. Exploiting bacteria for cancer immunotherapy. *Nat Rev Clin Oncol*. 2024;21(8):569–589. doi:10.1038/s41571-024-00908-9
36. Wang Y, Guo W, Wu X, et al. Oncolytic Bacteria and their potential role in bacterium-mediated tumour therapy: a conceptual analysis. *J Cancer*. 2019;10(19):4442–4454. doi:10.7150/jca.35648
37. Yang M, Zhong P, Wei P. Living bacteria: a new vehicle for vaccine delivery in cancer immunotherapy. *Int J Mol Sci*. 2025;26(5):2056. doi:10.3390/ijms26052056
38. Redenti A, Im J, Redenti B, et al. Probiotic neoantigen delivery vectors for precision cancer immunotherapy. *Nature*. 2024;635(8038):453–461. doi:10.1038/s41586-024-08033-4
39. Liang K, Liu Q, Li P, et al. Endostatin gene therapy delivered by attenuated Salmonella typhimurium in murine tumor models. *Cancer Gene Ther*. 2018;25(7–8):167–183. doi:10.1038/s41417-018-0021-6
40. Vitiello M, Evangelista M, Di Lascio N, et al. Antitumoral effects of attenuated Listeria monocytogenes in a genetically engineered mouse model of melanoma. *Oncogene*. 2019;38(19):3756–3762. doi:10.1038/s41388-019-0681-1
41. Huang J, Wu Z, Xu J. Effects of biofilm nano-composite drugs OMVs-MSN-5-FU on cervical lymph node metastases from oral squamous cell carcinoma. *Front Oncol*. 2022;12:881910. doi:10.3389/fonc.2022.881910
42. Incir İ, Kaplan Ö. Escherichia coli in the production of biopharmaceuticals. *Biotechnol Appl Biochem*. 2025;72(2):528–541. doi:10.1002/bab.2664
43. Xiang S, Khan A, Yao Q, Wang D. Recent advances in bacterial outer membrane vesicles: effects on the immune system, mechanisms and their usage for tumor treatment. *J Pharm Anal*. 2024;14(12):101049. doi:10.1016/j.jpha.2024.101049
44. Li M, Zhou H, Yang C, et al. Bacterial outer membrane vesicles as a platform for biomedical applications: an update. *J Control Release*. 2020;323:253–268. doi:10.1016/j.jconrel.2020.04.031
45. Li Y, Ma X, Yue Y, et al. Rapid surface display of mRNA antigens by bacteria-derived outer membrane vesicles for a personalized tumor vaccine. *Adv Mater*. 2022;34(20):e2109984. doi:10.1002/adma.202109984
46. Shi J, Ma Z, Pan H, et al. Biofilm-encapsulated nano drug delivery system for the treatment of colon cancer. *J Microencapsul*. 2020;37(7):481–491. doi:10.1080/02652048.2020.1797914
47. Cheng CM, Lu YL, Chuang KH, et al. Tumor-targeting prodrug-activating bacteria for cancer therapy. *Cancer Genet Ther*. 2008;15(6):393–401. doi:10.1038/cgt.2008.10
48. Younis MA, Khalil IA, Elewa YHA, Kon Y, Harashima H. Ultra-small lipid nanoparticles encapsulating sorafenib and midkine-siRNA selectively-eradicate sorafenib-resistant hepatocellular carcinoma in vivo. *J Control Release*. 2021;331:335–349. doi:10.1016/j.jconrel.2021.01.021

49. Ji Y, Hao J, Tao X, Li Z, Chen L, Qu N. Preparation and anti-tumor activity of paclitaxel silk protein nanoparticles encapsulated by biofilm. *Pharm Dev Technol*. 2024;29(6):627–638. doi:10.1080/10837450.2024.2376075
50. Kong Q, Six DA, Liu Q, et al. Phosphate groups of lipid A are essential for Salmonella enterica serovar Typhimurium virulence and affect innate and adaptive immunity. *Infect Immun*. 2012;80(9):3215–3224. doi:10.1128/IAI.00123-12
51. Kong Q, Yang J, Liu Q, Alamuri P, Roland KL, Curtiss R. Effect of deletion of genes involved in lipopolysaccharide core and O-antigen synthesis on virulence and immunogenicity of Salmonella enterica serovar typhimurium. *Infect Immun*. 2011;79(10):4227–4423. doi:10.1128/IAI.05398-11